Published in "Physical Review B - Condensed Matter and Materials Physics
86(7): 075130 , 2012"
which should be cited to refer to this work.

Rubidium superoxide: A *p*-electron Mott insulator

Roman Kováčik,[1,*] Philipp Werner,[2] Krzysztof Dymkowski,[3,†] and Claude Ederer[3,‡]
[1]*Peter Grünberg Institut and Institute for Advanced Simulation, Forschungszentrum Jülich and JARA, 52425 Jülich, Germany*
[2]*Department of Physics, University of Fribourg, Ch. du Musée 3, 1700 Fribourg, Switzerland*
[3]*Materials Theory, ETH Zürich, Wolfgang-Pauli-Strasse 27, 8093 Zürich, Switzerland*

Rubidium superoxide, RbO_2, is a rare example of a solid with partially filled electronic p states, which allows us to study the interplay of spin and orbital order and other effects of strong electronic correlations in a material that is quite different from the conventional d or f electron systems. Here we show, using a combination of density functional theory (DFT) and dynamical mean-field theory, that at room temperature RbO_2 is indeed a paramagnetic Mott insulator. We construct the metal-insulator phase diagram as a function of temperature and Hubbard interaction parameters U and J. Due to the strong particle-hole asymmetry of the RbO_2 band structure, we find strong differences compared to a simple semielliptical density of states, which is often used to study the multiband Hubbard model. In agreement with our previous DFT study, we also find indications for complex spin and orbital order at low temperatures.

I. INTRODUCTION

Rubidium superoxide, RbO_2, is an interesting example of a material where spin and orbital order appears not as a result of partially filled d or f states, but due to partially filled p electron states. RbO_2 is a member of the family of alkali superoxides AO_2 (A = K, Rb, or Cs), which are insulating crystalline materials composed of A^+ and $(O_2)^-$ ions.[1,2] At room temperature, RbO_2 has a tetragonal crystal structure [see Fig. 1(a)], while with decreasing temperature this structure undergoes several weak distortions, first to orthorhombic, then to monoclinic symmetry.[2,3] The electronic structure around the Fermi level is dominated by oxygen p states which can be well approximated by molecular orbitals (MOs) corresponding to the O_2 units, and are filled with 9 electrons [see Fig. 1(b)]. Assuming no further symmetry breaking, the two highest occupied antibonding π^* orbitals are 3/4 filled.

The degeneracy of these orbitals can be lifted through either magnetic or orbital long-range order, or both. The alkali superoxides thus allow us to study "correlation effects" in a completely different class of materials compared to the more conventional transition-metal oxides or f-electron systems. Antiferromagnetic order is indeed found experimentally at low temperatures [$T_N(RbO_2) \approx 15$ K],[1,2] and it was suggested by recent density functional theory (DFT) and model studies that the insulating character of alkali superoxides at low temperatures can be explained by the interplay of correlation effects (spin and orbital order) and crystal distortions.[4–9] However, the nature of the insulating state of these superoxides at room temperature has so far remained unexplored.

Due to the high-symmetry crystal structure with no long-range order of spins or orbitals, it is impossible to explain the insulating character of the alkali superoxides at room temperature within an effective single particle band picture. Here we show, using a combination of DFT and dynamical mean-field theory (DFT + DMFT), that RbO_2 at room temperature is in fact a *Mott insulator*, where the strong Coulomb repulsion prevents the electron hopping between adjacent sites.

II. ELECTRONIC STRUCTURE OF RbO_2

We obtain the electronic structure of RbO_2 in the high-symmetry tetragonal structure from a non-spin-polarized DFT calculation using the Quantum-ESPRESSO package,[10] employing the generalized gradient approximation (GGA) of Perdew, Burke, and Ernzerhof[11] and ultrasoft pseudopotentials.[12] We use lattice parameters $a = 4.20$ Å, $c = 7.07$ Å, and an O-O bond length $d_{O-O} = 1.36$ Å, determined in Ref. 4.

Figures 2(a) and 2(b) show the resulting density of states (DOS) and band structure. It can be seen that the electronic structure of RbO_2 indeed closely resembles the simple MO picture sketched in Fig. 1(b), with a splitting of about 5 eV between the bonding and antibonding π and π^* bands, and a single band corresponding to bonding σ MOs at -6 eV. The antibonding σ^* states at $\sim$5 eV are strongly intermixed with other empty states corresponding to the Rb^+ cations.

In the following we will focus only on the partially filled antibonding π^* bands [highlighted in Fig. 2(b)], which we represent in a basis of O_2 bond-centered maximally localized Wannier functions (MLWFs).[13] The hopping parameters associated with a tight-binding representation of the Hamiltonian in the basis of π^* MLWFs allow for a quantitative comparison of the band structure obtained in our study with similar reports in the literature (see Table I).

Our calculated parameters agree very well with the results of Ref. 7. The small quantitative difference is apparently due to a marginally larger bandwidth obtained in Ref. 7 using the local density approximation compared to our GGA results. The leading hopping parameters calculated in Ref. 5 for KO_2 are larger than the results for RbO_2, due to the smaller lattice parameters of KO_2, but exhibit the same overall trends. We also list previously unpublished hopping parameters, calculated for antiferromagnetic and ferromagnetic order of the O_2 magnetic moments in Ref. 4 (for RbO_2). It can be seen that the corresponding hopping amplitudes do not differ significantly from the nonmagnetic case considered here.

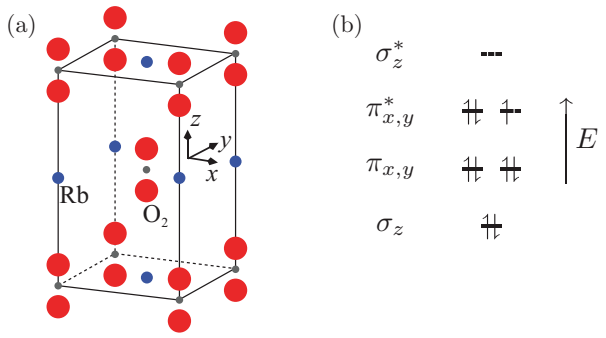

FIG. 1. (Color online) (a) Tetragonal crystal structure of RbO_2 at room temperature. (b) Electronic structure represented by a set of oxygen p molecular orbitals. (Adapted from Fig. 1 of Ref. 4.)

III. RbO_2 WITHIN DYNAMICAL MEAN-FIELD THEORY

A. Computational method

To calculate the electronic properties at finite temperature and account for local correlation effects, we use dynamical mean-field theory[14] (DMFT) which allows us to map the lattice problem to an effective problem of a single-site impurity surrounded by a bath. The interaction part of the impurity Hamiltonian is taken to be of the Slater-Kanamori form

$$\begin{aligned} H_{\rm int} = & \sum_a U n_{a,\uparrow} n_{a,\downarrow} + \sum_{a\neq b,\sigma} U' n_{a,\sigma} n_{b,-\sigma} \\ & + \sum_{a\neq b,\sigma} (U'-J) n_{a,\sigma} n_{b,\sigma} \\ & - \sum_{a\neq b} J(d^\dagger_{a,\downarrow} d^\dagger_{b,\uparrow} d_{b,\downarrow} d_{a,\uparrow} + d^\dagger_{b,\uparrow} d^\dagger_{b,\downarrow} d_{a,\uparrow} d_{a,\downarrow} + \text{H.c.}), \end{aligned} \tag{1}$$

with $d^\dagger_{a,\sigma}$ the creation operator for an electron of spin σ in orbital a, $n_{a,\sigma} = d^\dagger_{a,\sigma} d_{a,\sigma}$, and $U' = U - 2J$. To solve the effective impurity problem, we use the strong-coupling continuous time quantum Monte Carlo approach (CT-HYB).[15,16] From the self-consistently determined hybridization function $\Delta(\tau)$, the impurity Green's function $G_{\rm imp}(\tau)$ is computed and measured on a homogeneous grid of $N_\tau = 1000 \times [\sqrt{\beta/40\ \text{eV}^{-1}}]$ points, where $[\ldots]$ represents the nearest integer number. After Fourier transformation we obtain the self-energy in Matsubara space,

$$\Sigma(i\omega_n) = i\omega_n + \mu - G^{-1}_{\rm imp}(i\omega_n) - \Delta(i\omega_n), \tag{2}$$

where $\omega_n = (2n+1)\pi/\beta$ for integer n, μ is the chemical potential, and $\beta = 1/(k_B T)$ the inverse temperature. Using this self-energy and the single-particle Hamiltonian $H(\mathbf{k})$ we obtain the local lattice Green's function by averaging over the Brillouin zone:

$$G_{\rm loc}(i\omega_n) = \frac{1}{N_k} \sum_{\mathbf{k}} [i\omega_n + \mu - H(\mathbf{k}) - \Sigma(i\omega_n)]^{-1}. \tag{3}$$

The DMFT self-consistency condition demands that this local lattice Green's function is the same as the impurity Green's function. This condition, in combination with Eq. (2), yields the hybridization function for the next DMFT iteration,

$$\Delta(i\omega_n) = i\omega_n + \mu - G^{-1}_{\rm loc}(i\omega_n) - \Sigma(i\omega_n). \tag{4}$$

We only include the partially filled antibonding $\pi^*_{x/y}$ bands in our DMFT calculations for RbO_2, and express the corresponding Hamiltonian $H(\mathbf{k})$ in the basis of O_2 bond-centered MLWFs discussed in Sec. II. We note that we use the full *ab initio* Hamiltonian as input for the DMFT calculation, not just a simplified tight-binding model based on the most dominant hopping amplitudes (like, e.g., the ones listed in Table I). The corresponding DOS is shown in Fig. 2(c). One can recognize a pronounced asymmetry with respect to half filling. In DMFT studies, a model semicircle (SC) density of states (DOS) is often employed to represent the electronic bands, since it leads to a simple expression connecting Δ and $G_{\rm imp}$. Furthermore, due to the resulting particle-hole symmetry, only occupations between zero and half filling need to be studied. Here, we investigate the differences between results obtained using the model SC DOS and the realistic DFT band structure of RbO_2 in the tetragonal crystal structure. The bandwidth of

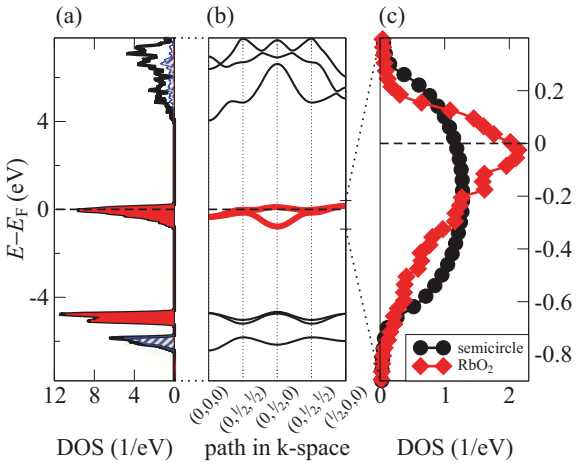

FIG. 2. (Color online) Density of states (DOS) (a) and band structure (b) of nonmagnetic RbO_2. In (a) the total DOS is shown as thick (black) line, while the projection on O_2 σ and π states is shown as (blue) striped and (red) filled areas, respectively. Panel (c) shows the DOS (per spin orbital) of the π^* bands used in the DMFT calculations, compared to a semicircular DOS with the same bandwidth (a small broadening is applied in both cases).

TABLE I. Hopping amplitudes h^R_{ij} (in meV) corresponding to π^* MLWFs i and j, along the crystal direction R. The first 3 columns correspond to nonmagnetic (NM) results obtained in the present study, in Ref. 7, and in Ref. 5, respectively. In the last 4 columns, we show unpublished data from our previous study (Ref. 4) for antiferromagnetic (AFM) and ferromagnetic (FM) order. The (local) majority/minority spin channels are denoted as ↑/↓.

	NM			AFM(↑/↓)		FM(↑/↓)	
	RbO_2		KO_2	RbO_2			
$h^{(111)/2}_{xx}$	−32	−34	−51	−33	−33	−30	−36
$h^{(111)/2}_{xy}$	−56	−60	−98	−58	−58	−52	−64
$h^{(100)}_{xx}$	50	54	106	45	58	45	58
$h^{(100)}_{yy}$	12	16	−1	11	14	12	14
$h^{(110)}_{xx/xy}$	−12		−11	−11	−14	−11	−14
$h^{(001)}_{xx}$	−8		−13	−7	−10	−7	−8

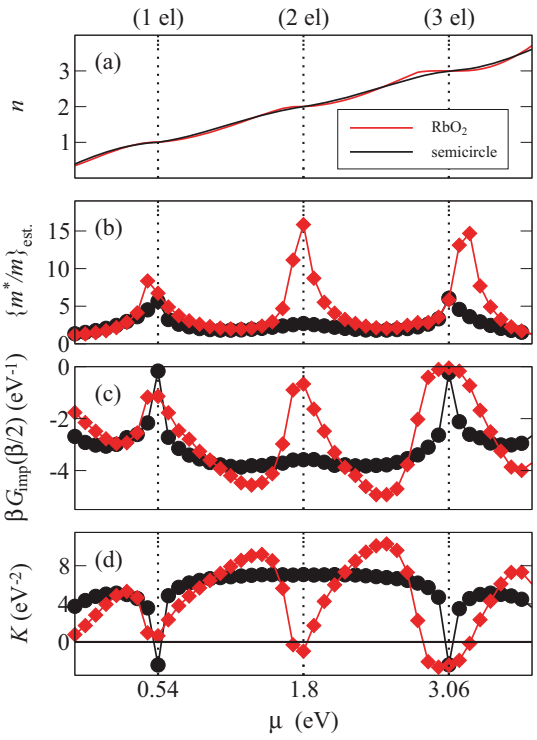

FIG. 3. (Color online) Various quantities evaluated from the impurity Green's function indicating the metal-insulator transition at integer filling, calculated for $\beta = 40\,\mathrm{eV}^{-1}$ ($T \approx 290$ K), $U = 1.2$ eV, and $J = 0.0$ eV. The average over all spin orbitals is shown in panels (b), (c), and (d).

the SC DOS is set equal to the bandwidth of the RbO_2 DOS [0.93 eV; see Fig. 2(c)].

B. Room temperature results

Generally, the value of the spectral function at zero energy indicates whether a material is insulating or metallic. However, obtaining the spectral function from the imaginary time Green's function requires an analytic continuation to the real axis, which can introduce additional uncertainties.[17] We therefore consider several possible indicators for the metal-insulator transition (MIT) which are directly accessible from $G_{\mathrm{imp}}(\tau)$. All of these quantities (described in more detail below) are compared in Fig. 3, calculated at room temperature ($\beta = 40\ \mathrm{eV}^{-1}$) for interaction parameters close to the MIT ($U = 1.2$ eV and $J = 0$).

One possibility is to monitor the occupation $n = -\sum_\alpha G^\alpha_{\mathrm{imp}}(\beta)$ (α is the spin-orbital index) as a function of the chemical potential μ [see Fig. 3(a)] and to identify the insulating phase by a plateau in $n(\mu)$. This, however, requires a large number of calculations for slightly different values of μ. Another indicator is given by the mass enhancement in the low-temperature metallic phase, which grows rapidly as the Mott insulating state is approached, and which we estimate from the self-energy at the lowest Matsubara frequency (see Ref. 18):

$$\left\{\frac{m^*}{m}\right\}_{\mathrm{est.}} = 1 - \frac{\Im[\Sigma(i\omega_0)]}{\omega_0}. \qquad (5)$$

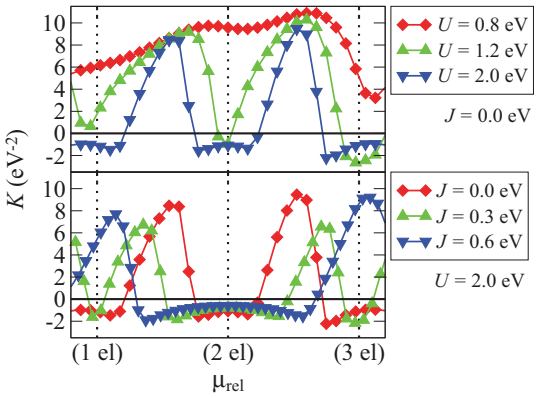

FIG. 4. (Color online) Slope K for RbO_2 input and selected values of U and J at $\beta = 40\ \mathrm{eV}^{-1}$ (average over all spin-orbitals is shown).

We also consider the following estimate of the spectral function (see, e.g., Ref. 18):

$$A(0) \approx -\frac{\beta}{\pi} G_{\mathrm{imp}}\left(\frac{\beta}{2}\right). \qquad (6)$$

While for both of these quantities [shown in Figs. 3(b) and 3(c), respectively] only one calculation at the correct μ value is required, the identification of the MIT phase boundary requires the definition of a suitable threshold value. In addition, $G(\beta/2)$ suffers from significant statistical noise in the insulating state, as this τ region is difficult to sample with standard CT-HYB. A quantity which is quite insensitive to noise is the slope of $G_{\mathrm{imp}}(i\omega \to 0)$, which is positive/negative for the metallic/insulating state.[18] In practice, we estimate the slope K from $G_{\mathrm{imp}}(i\omega)$ at the two lowest Matsubara frequencies:

$$K = \left\{\frac{\mathrm{d}\Im[G_{\mathrm{imp}}(0)]}{\mathrm{d}\omega}\right\}_{\mathrm{est.}} = \frac{\Im[G_{\mathrm{imp}}(i\omega_1) - G_{\mathrm{imp}}(i\omega_0)]}{\omega_1 - \omega_0}. \qquad (7)$$

In Fig. 3, a clear difference can be seen between the SC and the RbO_2 input. For the SC, the insulating state already appears at 1 and 3 el filling, while 2 el filling is clearly metallic. In contrast, the RbO_2 electronic structure yields a clear insulating state at 3 el filling and a (just barely) insulating state at 2 el filling, while 1 el filling is still metallic. The different range of μ which leads to the insulating state for SC and RbO_2, respectively, indicates a sizable shift of the corresponding MIT boundary. The particle-hole asymmetry in the real electronic structure of RbO_2 thus leads to large quantitative changes compared to the simple SC DOS.

Figure 4 shows the slope K for different values of U and J at $T \approx 290$ K using the RbO_2 band structure. For fixed $J = 0$ eV, there is an obvious tendency towards the insulating state with increasing U for all integer fillings, as expected. However, at fixed $U = 2$ eV, increasing J favors the Mott insulator at half filling (2 el) but favors the metallic solution for 1 and 3 el fillings. This is consistent with previous discussions of multiorbital models:[19,20] In the large-U limit, the width of the "Mott plateau" in μ is given by $\Delta_n^{\mathrm{Mott}} = E_{n+1} + E_{n-1} - 2E_n$, with E_n denoting the lowest eigenvalue of the n-particle eigenstates of H_{int} [Eq. (1)].[19] In our two-orbital case this estimate yields $U - 3J$ for $n = 1$, 3 and $U + J$ for $n = 2$, in agreement with the observed dependence of the plateau

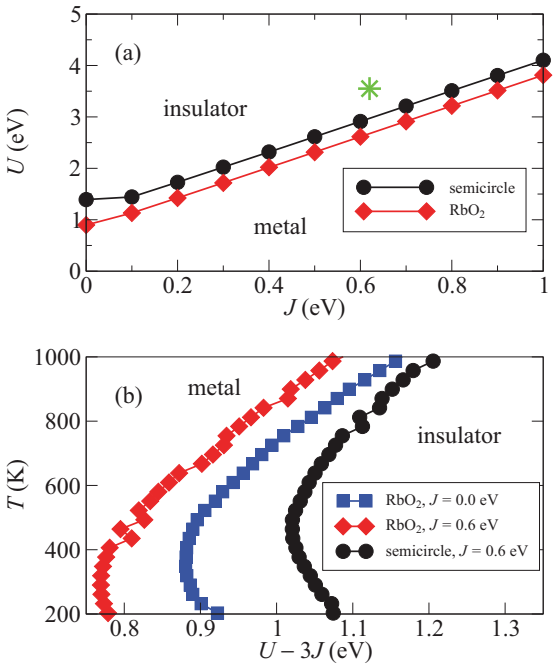

FIG. 5. (Color online) Metal-insulator phase diagrams. (a) Critical U as function of J at room temperature ($T \approx 290$ K). The green star indicates the realistic values for U and J calculated in Ref. 5. (b) Critical temperature as function of $U - 3J$.

width on J. In reality, the Mott plateau will be reduced by approximately the bandwidth W, so that we obtain the rough estimate

$$\Delta_3^{\text{Mott}} \approx U - 3J - W. \tag{8}$$

Based on the identification of the MIT boundary using the slope K, we computed the phase diagram for 3 el filling at room temperature ($T \approx 290$ K) as a function of the interaction parameters U and J [see Fig. 5(a)]. Since Δ^{Mott} must be larger than zero for a Mott insulating solution to exist, Eq. (8) also provides a crude estimate for the critical interaction strength: $U_c - 3J \approx W$. It can be seen that the MIT boundary in Fig. 5(a) agrees nicely with this simple estimate. Furthermore, the critical $U - 3J$ at room temperature differs by ≈30% of the bandwidth between RbO_2 and the simple SC DOS, and increases slightly as a function of T for $T \gtrapprox$ 300–400 K, while the opposite trend is observed at lower T [Fig. 5(b)].

For realistic values of the interaction parameters $U = 3.55$ eV and $J = 0.62$ eV, which were obtained for π^* orbitals in the very similar material KO_2 using the constrained LDA and random-phase approximation,[5] the insulating state is obtained for both SC and RbO_2. Our results therefore predict a Mott insulating state (without long-range order) for RbO_2 at room temperature, consistent with experimental observations.

We point out that it is in principle possible that dynamically fluctuating local structural distortions, without any long-range order, may eventually persist at elevated temperatures, similar to the dynamic Jahn-Teller distortion observed in $LaMnO_3$ above the orbital order transition temperature.[21,22] However, since such structural fluctuations are not included in our DMFT treatment, our results clearly demonstrate that they are not essential to explain the insulating nature of RbO_2 at room

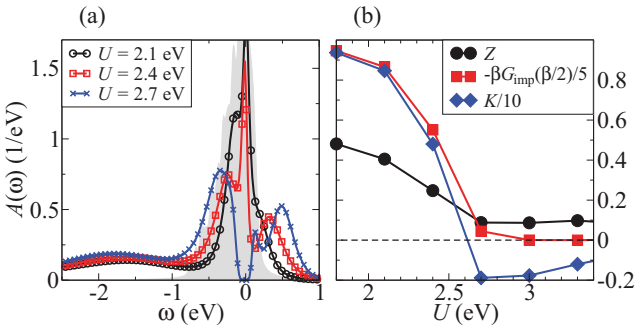

FIG. 6. (Color online) Spectral functions (a) and the various indicators for the MIT (b) for RbO_2 at $\beta = 40\,\text{eV}^{-1}$ ($T \approx 290$ K), $J = 0.6$ eV, and different values of U around the MIT. $Z = \{m^*/m\}^{-1}_{\text{est.}}$ and K is given in eV^{-2}. The noninteracting DOS is shown as grey shaded area in (a).

temperature. The Coulomb repulsion between electrons is sufficient to open up a gap in the spectral function (see also next paragraph) even in the ideal high-symmetry structure. Furthermore, the weak spin-orbit interaction, which was suggested to have an influence on the low-temperature ordered phase in the related material KO_2,[5,6] is not expected to have a significant effect on the insulating properties of RbO_2 at room temperature.

While we did not find evidence for a coexistence region, indicative of a first-order MIT, for $T \geqslant 145$ K, we have verified that we obtain an insulating state with a clear gap in the spectral function, even at room temperature. To demonstrate this, we have used the maximum entropy method[17] to construct spectral functions for RbO_2 (3 el filling) at $\beta = 40\,\text{eV}^{-1}$, $J = 0.6$ eV, and different values of U around the MIT. The result is shown in Fig. 6(a). A gap is present for $U \geqslant 2.7$ eV, in perfect agreement with the various indicators of the MIT discussed previously [and which are shown in Fig. 6(b)]. In agreement with Ref. 23 we find a "bad metal" region with a strongly renormalized $Z = \{m^*/m\}^{-1}_{\text{est.}} \lesssim 0.4$ in the vicinity of the Mott transition. From Fig. 6(a) it can be seen that this corresponds to spectral functions with substantial narrowing of the central quasiparticle feature and an emerging three-peak structure visible for $U = 2.4$ eV. In addition, there is a significant spectral weight transfer to energies around −2 eV compared to the noninteracting DOS.

C. Low-temperature behavior

Finally, we focus on the low-temperature behavior. While for temperatures $T \geqslant 200$ K (for which we did not find indications of ordered states), the hybridization function is averaged over all spin orbitals in each iteration of the DMFT self-consistency cycle, Fig. 7 shows the evolution of the occupation of each individual spin-orbital at $T \approx 29$ K when no such averaging is performed. While for some values of J the occupations eventually converge to spin and/or orbitally polarized states, the occupations exhibit characteristic oscillations for other values of J. As discussed in Ref. 24, such oscillations indicate that the system wants to adopt an ordered state with a sublattice structure that is incompatible with the

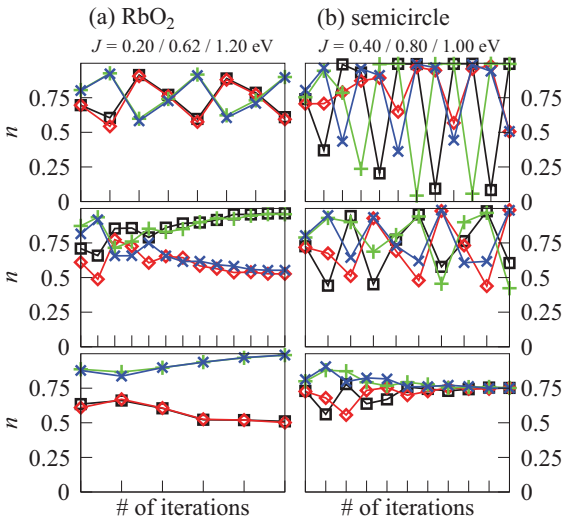

FIG. 7. (Color online) Evolution of individual occupations for different J and fixed $U - J = 2.93$ eV at $T \approx 29$ K for RbO_2 input (a) and for the SC DOS (b). (Black) Squares: orbital 1, spin up; (red) diamonds: orbital 2, spin up; (green) plus symbols: orbital 1, spin down; (blue) crosses: orbital 2, spin down.

applied self-consistency condition (in our case all sites are forced to be equivalent).

Even though we do not attempt to fully resolve the resulting spin and orbital patterns, we can make a number of interesting observations. First of all, there are drastic differences between RbO_2 [Fig. 7(a)] and the simple SC DOS [Fig. 7(b)]. The latter oscillates between three states with different spin and orbital polarization (SP and OP) and is insulating for $J \leqslant 0.8$ eV, while for higher J it is metallic with no SP and OP (in these calculations both U and J have been varied while keeping $U - J$ constant). For RbO_2 we can distinguish three different regimes [see Fig. 8(b)]: (i) For $J \leqslant 0.5$ eV, the occupation

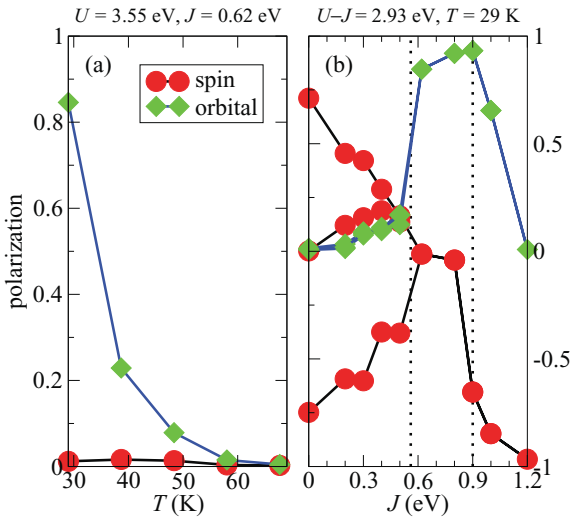

FIG. 8. (Color online) (a) Temperature dependence of spin and orbital polarization for fixed U and J. (b) spin and orbital polarization as a function of J for $U - J = 2.93$ eV and $T \approx 29$ K. All data correspond to RbO_2 input. The vertical dashed lines in (b) indicate boundaries between regions of qualitatively different behavior.

oscillates between three different states with different SP and almost no OP [see also upper panel of Fig. 7(a)], (ii) for $J = 0.62$ and 0.8 eV, a stable solution with large OP and zero SP appears [middle panel of Fig. 7(a)], while (iii) a further increase of J induces a stable SP and reduced OP [lower panel of Fig. 7(a)]. The system is insulating for all $J \leqslant 1.0$ eV, while for $J = 1.2$ eV it is a ferromagnetic half metal with full SP and no OP. In Fig. 8(a) we show the SP and OP of RbO_2 as a function of temperature for the realistic values $U = 3.55$ eV and $J = 0.62$ eV. The system is insulating and while essentially no SP develops down to $T \approx 30$ K, OP appears below $T \approx 60$ K and reaches almost its maximum at $T \approx 30$ K. While it is not possible from our calculations to make a prediction about the character of the expected spin- and orbitally-ordered ground state, the above temperatures are consistent with our previous estimate of the ordering temperature based on total energy differences of different orbitally ordered configurations obtained from GGA+U calculations at $T = 0$ K.[4] Furthermore, we note that the specific character of the low-temperature ordered state is expected to be strongly influenced by structural distortions, such as, e.g., a tilting of the oxygen molecules away from the tetragonal axis.[6,8]

IV. SUMMARY AND CONCLUSIONS

In summary our calculations clearly show that for realistic values of the interaction parameters U and J, RbO_2 at room temperature is a paramagnetic Mott insulator without exhibiting any symmetry-breaking long-range order. Furthermore we show that the insulating state is obtained without the need to include dynamic distortions of the high-symmetry tetragonal structure. We find pronounced *quantitative* differences between the widely used SC DOS and the realistic electronic structure of RbO_2, which leads to a strong asymmetry between the 1/4-filled and 3/4-filled cases. We also find indications of complex spin and orbital order below $T \approx 30$ K, the character of which seems to depend strongly on J. Furthermore, at low temperature RbO_2 exhibits clear *qualitative* differences compared to the simplified SC DOS. It will be interesting to clarify in future work whether single-site DMFT is capable of resolving the complicated spin and orbital patterns predicted within model calculations based on a perturbative treatment of electron-electron interaction and a simplified electronic structure of RbO_2.[7,9] Finally, our study demonstrates that the same physics that is usually associated with transition-metal oxides and f-electron materials also governs the properties of the otherwise rather different alkali superoxides. These materials thus provide an interesting opportunity to study the "Mott physics" of a degenerate two-band system.

ACKNOWLEDGMENTS

The authors are indebted to Emanuel Gull for his help with the installation and general use of the CT-HYB code. This work was done mostly within the School of Physics at Trinity College Dublin, supported by Science Foundation Ireland under Ref. SFI-07/YI2/I1051, and made use of computational facilities provided by the Trinity Centre for High Performance Computing.

*r.kovacik@fz-juelich.de; previous address: School of Physics, Trinity College Dublin, Dublin 2, Ireland.
†Previous address: School of Physics, Trinity College Dublin, Dublin 2, Ireland.
‡claude.ederer@mat.ethz.ch; previous address: School of Physics, Trinity College Dublin, Dublin 2, Ireland.

[1] A. Zumsteg, M. Ziegler, W. Känzig, and M. Bösch, Phys. Condens. Matter **17**, 267 (1974).
[2] M. Labhart, D. Raoux, W. Känzig, and M. A. Bösch, Phys. Rev. B **20**, 53 (1979).
[3] M. Rosenfeld, M. Ziegler, and W. Känzig, Helv. Phys. Acta **51**, 298 (1978).
[4] R. Kováčik and C. Ederer, Phys. Rev. B **80**, 140411 (2009).
[5] I. V. Solovyev, New J. Phys. **10**, 013035 (2008).
[6] M. Kim, B. H. Kim, H. C. Choi, and B. I. Min, Phys. Rev. B **81**, 100409 (2010).
[7] E. R. Ylvisaker, R. R. P. Singh, and W. E. Pickett, Phys. Rev. B **81**, 180405 (2010).
[8] A. K. Nandy, P. Mahadevan, P. Sen, and D. D. Sarma, Phys. Rev. Lett. **105**, 056403 (2010).
[9] K. Wohlfeld, M. Daghofer, and A. M. Oleś, EPL **96**, 27001 (2011).
[10] P. Gianozzi, S. Baroni, N. Bonini, M. Calandra, R. Car, C. Cavazzoni, D. Ceresoli, G. L. Chiarotti, M. Cococcioni, I. Dabo *et al.*, J. Phys.: Condens. Matter **21**, 395502 (2009).
[11] J. P. Perdew, K. Burke, and M. Ernzerhof, Phys. Rev. Lett. **77**, 3865 (1996).
[12] D. Vanderbilt, Phys. Rev. B **41**, 7892 (1990).
[13] A. A. Mostofi, J. R. Yates, Y.-S. Lee, I. Souza, D. Vanderbilt, and N. Marzari, Comput. Phys. Commun. **178**, 685 (2008).
[14] A. Georges, G. Kotliar, W. Krauth, and M. J. Rozenberg, Rev. Mod. Phys. **68**, 13 (1996).
[15] P. Werner and A. J. Millis, Phys. Rev. B **74**, 155107 (2006).
[16] E. Gull, A. J. Millis, A. I. Lichtenstein, A. N. Rubtsov, M. Troyer, and P. Werner, Rev. Mod. Phys. **83**, 349 (2011).
[17] M. Jarrell and J. E. Gubernatis, Phys. Rep. **269**, 133 (1996).
[18] S. Fuchs, E. Gull, M. Troyer, M. Jarrell, and T. Pruschke, Phys. Rev. B **83**, 235113 (2011).
[19] P. Werner, E. Gull, and A. J. Millis, Phys. Rev. B **79**, 115119 (2009).
[20] L. de' Medici, Phys. Rev. B **83**, 205112 (2011).
[21] M. C. Sánchez, G. Subías, J. García, and J. Blasco, Phys. Rev. Lett. **90**, 045503 (2003).
[22] X. Qiu, T. Proffen, J. F. Mitchell, and S. J. L. Billinge, Phys. Rev. Lett. **94**, 177203 (2005).
[23] L. de' Medici, J. Mravlje, and A. Georges, Phys. Rev. Lett. **107**, 256401 (2011).
[24] C.-K. Chan, P. Werner, and A. J. Millis, Phys. Rev. B **80**, 235114 (2009).